Quantitating intracellular transport of polyplexes by spatio-temporal image correlation spectroscopy

Rajan P. Kulkarni*†, David D. Wu†‡, Mark E. Davis§¶, and Scott E. Fraser*†‡¶

*Option in Biochemistry and Molecular Biophysics, †Division of Biology, §Division of Chemistry and Chemical Engineering, and ‡Option in Bioengineering, California Institute of Technology, Pasadena, CA 91125

Communicated by Robert Langer, Massachusetts Institute of Technology, Cambridge, MA, March 9, 2005 (received for review September 15, 2004)

Quantitatively understanding how nonviral gene delivery vectors (polyplexes) are transported inside cells is essential before they can be optimized for gene therapy and medical applications. In this study, we used spatio-temporal image correlation spectroscopy (ICS) to follow polymer-nucleic acid particles (polyplexes) of various sizes and analyze their diffusive-like and flow behaviors intracellularly to elucidate the mechanisms responsible for their transport. ICS is a quantitative imaging technique that allows the assessment of particle motion in complex systems, although it has not been widely used to date. We find that the internalized polyplexes are able to use microtubule motors for intracellular trafficking and exhibit different transport behaviors for short (<10 s) versus long (≈60 s) correlation times. This motion can be explained by a memory effect of the microtubule motors. These results reveal that, although microtubule motor biases may be present for short periods of time, resulting in a net directional velocity, the overall long-term motion of the polyplexes is best described as a random walk-like process. These studies suggest that spatio-temporal ICS is a powerful technique for assessing the nature of intracellular motion and provides a quantitative tool to compare the transport of different objects within a living cell.

transfection agent | molecular mobility | cytoplasmic crowding | cyclodextrin

Recently, significant progress has been made in developing alternatives to viral-based gene therapy, motivated by safety concerns of viral infection. Understanding such nonviral gene delivery (one type of vector that involves the combination of synthetic polymers and nucleic acids to form particles called polyplexes and is used here) requires knowledge of how they behave within cells, including the mechanisms involved in polyplex trafficking such as endocytosis, cytoplasmic transport, endosomal escape, and nuclear localization (1–3). Recent reports have indicated the presence of significant bottlenecks in the delivery process, especially problems with endosomal escape (4). Measuring these dynamics, especially transport parameters, is important for understanding both how such delivery methods compare with viruses and how to improve their efficiencies.

Confocal microscopy allows for good visualization of small quantities of fluorescently labeled species. However, only a few studies of cytoplasmic transport have focused on quantitative biophysical parameters such as effective diffusion constants or transport velocities (4–6). Most experiments measuring these parameters have focused on examining small injected oligonucleotides or proteins (7–11). In contrast, polyplexes that range in size from 75 to 250 nm or larger enter cells by endocytosis and become enclosed in endosomes (12). For transport of large entities (>30 nm), such as the polyplexes used for gene therapy, issues such as crowding and microtubule transport become critical (13, 14).

Here, we describe spatio-temporal image correlation spectroscopy (ICS), a technique for characterizing the behavior of polyplexes and other subcellular particles. ICS, as first described by Petersen *et al.* (15), is an imaging corollary to fluorescence correlation spectroscopy (FCS). FCS, as initially detailed by Magde and coworkers (16–18), involved measuring the statistical fluctuation in the fluorescence signal at a single point as molecules passed through a fixed laser beam; dynamical information was obtained from these fluctuations. FCS has recently been used to measure diffusion constants of small proteins both in the cell membrane and cytoplasm (19–22); it works well for measuring rapid processes occurring on the microsecond to millisecond time scale. In contrast, ICS is useful for measuring processes occurring on a slower time scale (seconds to minutes) for spatially distinct objects, such as polyplexes within the cell.

In spatio-temporal ICS, a scanning laser beam (usually within a confocal microscope) is used to measure the fluorescence intensities of objects within a cell (15, 23, 24). The intensity information from each pixel in the image is then used to calculate the autocorrelation functions. Diffusion and flow information about an entire image plane, rather than just a fixed point, can be obtained with this method. ICS can provide quantitative information about objects smaller than the optical diffraction limit; however, such objects must be identifiable as discrete puncta for optimal performance. A major benefit of this technique is that it provides information about aggregate behavior in a region of interest by measuring statistical fluctuations. Previous studies have used ICS to determine the number of receptors on a cell surface and their degree of aggregation (25, 26). These original implementations of ICS did not include a temporal component. More recently, Srivastava and Petersen (27) and Wiseman *et al.* (28, 29) have described combined temporal and spatial autocorrelations. Although these studies have focused on model systems such as beads, the authors suggested that the method can be extended to analyze cytoplasmic dynamics. Here, we have successfully extended this methodology for live intracellular imaging studies.

We have measured the effective diffusion constants and transport velocities of polyplexes to understand how they behave when introduced to cells, specifically, how they are transported intracellularly. Our method allows us to continuously monitor intracellular polyplex behavior for up to 5 min. Polyplexes have quantitatively different behaviors for short correlation times (<10 s) than for longer correlation times. For short intervals, the motion of the polyplex is highly correlated and it has a pronounced memory effect (it continues to move along the same straight path as in the previous time step). For longer intervals, the memory effect is lost, and the motions can best be described as a random walk. These behaviors can be thought of in terms of the action and processivity of the microtubule motors (kinesin and dynein) that transport endosomal cargo through the cell. This study demonstrates the potential of spatio-temporal ICS for analyzing aspects of intracellular dynamics, which ultimately will be be important for monitoring and assessing the efficacy of cellular delivery agents.

Abbreviations: ICS, image correlation spectroscopy; CD, cyclodextrin; PEI, polyethyleneimine.

¶To whom correspondence may be addressed. E-mail: mdavis@cheme.caltech.edu or sefraser@caltech.edu.

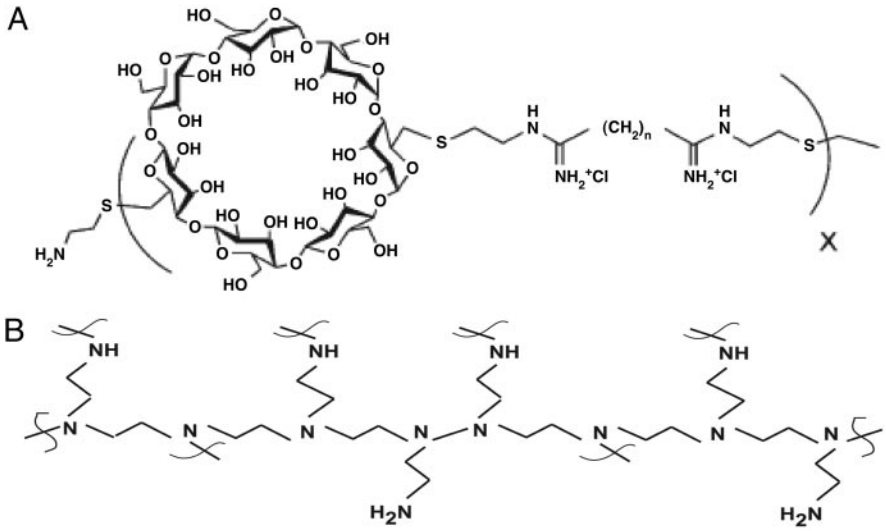

Fig. 1. Chemical structures for β-CD (*A*) and PEI (*B*) polymers used for complexing with DNA to create the nanometer-size polyplexes of interest. The PEI is a highly branched polymer with many free amino groups, as illustrated in the structure, whereas the CD has a small cavity created by the cyclized sugar moieties.

Materials and Methods

Cells. HeLa cells were grown in 10-cm culture dishes (Becton Dickinson) at 37°C in a humid 5% CO_2 atmosphere. Each dish held 10 ml of growth media (DMEM with 10% FBS, 100 units/ml of penicillin, 100 units/ml of streptomycin, 10 mM Hepes, 0.1 mM nonessential amino acids, and 2 mM L-glutamine; Irvine Scientific). The cells were passaged once a week and plated onto coverslip-bottom tissue culture plates (Lab-Tek) for imaging experiments (1.5 ml per well). Cells were incubated for 24 h before transfection. Cells were imaged 2 h after polyplex transfection.

Fluorescent Microsphere Preparation. Green fluorescent microspheres of sizes 200 nm, 500 nm, 1 μm, and 2 μm (FluoSpheres, Molecular Probes) were diluted 1:100 in either pure water or a 50% glycerol solution, placed onto a coverslip (50 μl), and imaged on the confocal microscope.

DNA Polyplexes. See Fig. 1 for schematic illustration of the chemical structures of the polymers. β-cyclodextrin (CD)-containing polymers were synthesized as described (30). The polymers were modified with adamantane-PEG 5000 to prevent particle aggregation in the presence of salt (30). Adamantane is a small hydrophobic molecule that associates with the CD by forming an inclusion compound within the hydrophobic cavity. Without adamantane-polyethylene glycol modification, the polyplexes aggregate excessively in solution (30). All DNA used to generate polyplexes was fluorescently labeled with Cy5 dye. To form β-CD polymer/DNA polyplexes, equal volumes of a 1 mg/ml β-CD polymer solution and a 0.1 mg/ml Cy5-labeled oligonucleotide solution (both in H_2O) were incubated at room temperature for 30 min. The 25-kDa branched polyethyleneimine (PEI)/DNA polyplexes were formulated similarly. Equal volumes of a 0.067 mg/ml of PEI solution and 0.1 mg/ml of Cy5-oligo solution (both in 20 mM Hepes, 50 mg/ml glucose) were incubated at room temperature for 30 min. Subsequently, 2 μl of 20 mg/ml of mPEG5000-SPA (in H_2O) was added and allowed to incubate at room temperature for another 15 min. Both the β-CD/DNA and PEI/DNA complexes had a 5:1 nitrogen/phosphate ratio. The size of the polyplexes (dependent on the concentrations of precursor and DNA) was measured by dynamic light scattering (Brookhaven Instruments, Holtsville, NY). The sizes of 80, 100, 180, and 220 nm are the effective mean diameters (by dynamic light scattering) of four different samples of monodisperse polyplexes, with variance of 3% or less. Both the polyethylene glycolylated β-CD/DNA and PEI/DNA polyplexes have been shown to enter and move within cells as nonaggregated particles by transmission electron microscopy studies (30).

Fluorescence Microscopy. An inverted Zeiss LSM 510 META confocal microscope was used for all fluorescence and bright-field measurements. Scan parameters (pixel time, scan area, and laser intensity) were varied to maximize the signal-to-noise ratio while minimizing frame time. Excitation of the green fluorescent microspheres was achieved with the 488-nm line of the argon ion laser, and excitation of Cy5 was achieved with the 633-nm He-Ne laser line. The fluorescence signal was detected through a variable confocal pinhole set to 1.5 Airy units, which was chosen to maximize the signal-to-noise ratio while minimizing out-of-plane light. At least 300 consecutive images were taken of each cell, with individual image frame rates varying between 1 and 2 Hz.

Spatio-Temporal Image Autocorrelation Methods and Analysis. Complete theoretical details of ICS, including equations, are given in *Supporting Methods*, which is published as supporting information on the PNAS web site. The z-direction point spread function was determined by taking a z-stack of 100-nm-diameter fluorescent microspheres. Fluorophore photobleaching (from continuous laser excitation) limited the maximum continuous observation times to 3–5 min; these times can be extended by using pauses in laser illumination when scanning. No specific correction for photobleaching was performed for these data series.

ICS analysis was performed as described in *Supporting Methods*. Images were manually thresholded by inspection to reduce the background contribution to the average intensity terms. Spatial autocorrelation functions for the images in each fluorescence time series were then calculated by using Eq. **S2a** from *Supporting Methods*. The spatial component of these correlation functions were then averaged and fit by nonlinear least squares by using Eq. **S4** from *Supporting Methods* to obtain the value for the beam radius. Next, the temporal correlation functions were separately calculated by using Eq. **S6** from *Supporting Methods*. These functions were then fit with either the diffusion (Eq. **S7** from *Supporting Methods*), diffusion plus flow (Eq. **S8** from *Supporting Methods*), or diffusion alternating with flow equa-

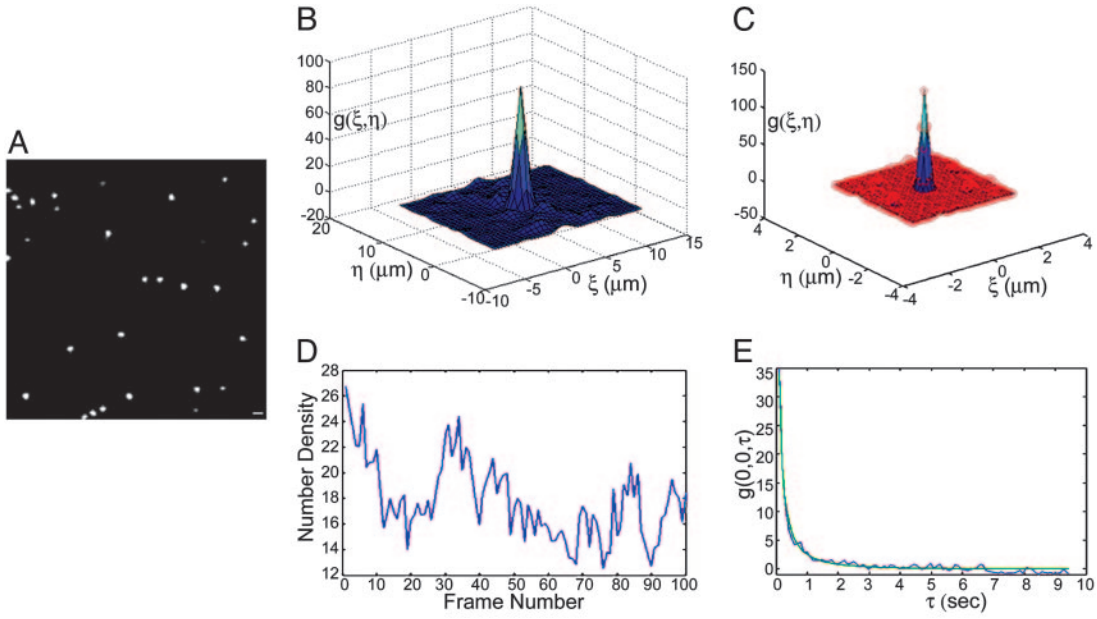

Fig. 2. Temporal image correlation analysis of 200-nm beads in a 50% glycerol solution. (*A*) The first figure from the time series of 300 images (captured at 10 Hz); 29 beads are present in this image. (Scale bar: 1 μm.) (*B*) The average spatial correlation analysis of the raw spatial correlations for each of the first 100 images from this time series is shown in blue. (*C*) The least-squares fit (shown by the red circles) of Eq. **S4** from *Supporting Methods*, to the spatial autocorrelation in *B*. The data are fit for η and ξ values from -2 to $+2$. (*D*) A graph of the number density of particles for the first 100 frames of the data set. The density values are within 10% of the values obtained by direct visualization (data not shown). (*E*) The least-squares fit of Eq. **S8** from *Supporting Methods* to the temporal autocorrelation curve of the data series. The diffusion coefficient for this curve is measured to be 2.62×10^{-9} cm^2/s, compared with the theoretical Stokes–Einstein value of 3.12×10^{-9} cm^2/s.

tions (Eq. **S9** from *Supporting Methods*). All calculations and fitting procedures were performed by using MATLAB software (Mathworks, Natick, MA).

Results and Discussion

Fluorescent Microsphere Images. The fidelity of our spatio-temporal ICS algorithms were validated by using fluorescent microspheres. By imaging microspheres (beads) of known sizes, the number density and diffusion coefficients of the beads can be measured to determine the accuracy of the number density algorithm and to compare the experimental diffusion values with those predicted by the Stokes–Einstein equation ($D = kT/6\pi\eta r$, where k is Boltzmann's constant, T is the temperature, η is the fluid viscosity, and r is the particle radius). Beads were placed in either pure water or a 50% glycerol solution. Fig. 2*A* shows a representative image from one of 25 experiments. Each sequence of images was processed to threshold detector noise (by manual inspection) and the spatial autocorrelation was determined (Fig. 2*B*). The autocorrelation curve was fit by using Eq. **S4** from *Supporting Methods*, and the number densities were calculated from the $g(0,0)$ value for each image (Fig. 2 *C* and *D*). In this example, ICS yields a number density of 27 beads from the spatial autocorrelation of Fig. 2*A*; a direct count indicated 29 beads in the image. The average error for 10 such data sets (25 frames each) was $6.3 \pm 2.5\%$; a sample analysis is shown in Fig. 5*A*, which is published as supporting information on the PNAS web site. Thus the number density yields a reasonable estimate of the number of beads in each image.

The next step was to validate the diffusion measurements from the temporal autocorrelation trace $g(0, 0, \tau)$. Eq. **S8** from *Supporting Methods* was used as the fit equation because there was a constant convective flow in the sample, yielding both effective diffusion and directed velocity terms. For these microspheres, the effective diffusion term corresponds to the classical diffusion constant for particles freely moving in a fluid and the velocity term is the velocity caused by convective flow. Fig. 5*B* shows the ICS determined experimental diffusion coefficients compared with theoretical values from the Stokes–Einstein equation ($n = 7$ samples each, SD $<10\%$ for each group); the experimental values are mostly within 10% of the predicted ones. Objects that diffuse with rates of 5×10^{-9} cm^2/s represent the effective maximum limit of the scanning spatio-temporal ICS method by using the setup described above, imaged at the maximum frame rate of 10 Hz. Fortunately, intracellular diffusive processes have been reported to be $\approx$2 orders of magnitude slower, making them suitable candidates for temporal ICS analysis.

Fluorescence Imaging of Polyplexes in HeLa Cells. To explore the intracellular motions of different sizes and types of polyplexes, both β-CD polyplexes with diameters of 80, 180, and 220 nm and PEI polyplexes of 100-nm diameter were analyzed; all polyplexes were complexed with Cy5-labeled oligonucleotides. Specifically, the cytoplasm was imaged continuously for at least 300 frames (corresponding to at least 100 s), and these images were used to determine polyplex transport parameters. This extended trajectory, which is at least five times longer than previous work (4), allows for a more detailed picture of the motions of these polyplexes as they travel through the cell and engage the transport networks to ultimately traffic to the perinuclear region.

As the polyplexes traveled through the cell, we noted that individual polyplexes mostly displayed confined motions in a small region of the cell (with particle trajectories confined to a 500-×-500-nm area) (31) or remained stationary over a 100-s trajectory. A few particles escaped these constraints and rapidly traveled through the cytoplasm in a correlated fashion, continuing along directed pathways with speeds of up to 0.5 μm/s. However, these correlated trajectories typically lasted for 10 s or less; afterward, the polyplexes displayed independent behavior and could even return to the starting position. A representative

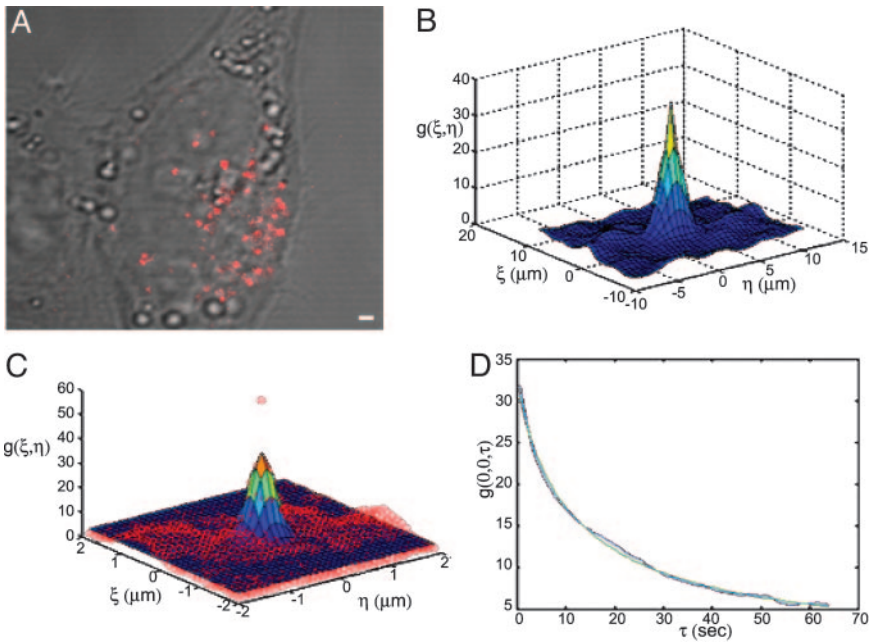

Fig. 3. An example of temporal ICS analysis of intracellular polyplexes. (*A*) A sample image of 100-nm PEI polyplexes inside a HeLa cell. The polyplexes are likely endosomally located and can be transported on microtubules (see text). The image series contains 200 images. (Scale bar: 1 μm.) (*B*) The raw average spatial correlation trace (shown in blue) for the first 100 images from *A*, taken at 1.25 Hz. (*C*) A Gaussian least-squares fit, depicted by red circles, to the data from *B*. η and ξ are evaluated from -2 to $+2$ for ease of calculation. (*D*) The temporal autocorrelation trace for the data in *B* and *C*. The green line is the best fit (by minimizing the residual, data not shown) by using the velocity plus diffusion equation (Eq. **S8** from *Supporting Methods*).

cell can be seen in Movie 1, which is published as supporting information on the PNAS web site; most particles appear to move very little. Occasionally a polyplex will travel quickly for a few seconds, then stall, and perhaps continue in a different direction; two such trajectories (of the cell depicted in Movie 1) are shown in Fig. 6, which is published as supporting information on the PNAS web site. In general, the trajectories appeared Brownian, with no preferred direction within the cell over this time scale. Similar behavior has been described by Lidke *et al.* (32) for endosomal trafficking of EGF-quantum dot complexes by microtubule-associated proteins (32). Given these random trajectories, it is not surprising that it usually takes 4–5 h for most polyplexes to reach the perinuclear region. In contrast, intracellular viral motion has been shown to often be directed toward the nucleus. For influenza virus, the individual viral particles reach the nucleus within 10 min of entering the cell because they directly engage the dynein motors (5).

Spatio-Temporal ICS Analysis. Spatio-temporal ICS was then used to analyze the aggregate diffusion-like and velocity characteristics of the polyplexes. As mentioned, the motion of the polyplexes empirically resembled a random walk process punctuated by occasional bursts of rapid, directed motion, suggesting the existence of a diffusive (stochastic) process with a putative velocity component throughout the entire trajectory (5). Of the temporal fit equations, Eqs. **S8** and **S9** in *Supporting Methods* yield both an effective diffusive term and an alternating velocity term. We fit the temporal autocorrelation curve with both equations to see whether both a diffusive term and a directed velocity value could be determined for the polyplexes. These values can ideally be used to characterize a cell's microtubule dynamics, because the microtubules and their motors are instrumental for endosomal trafficking (33–35). The velocity component may provide a measure of the activity of the microtubule motors as the polyplex cargoes are transported through the cytoplasm.

Correlation analysis involves examining the average of many simultaneous processes within a system. In this method, the motions of all particles within the region are considered simultaneously. Particles that appear to be temporarily immobile are included in the overall correlation function because they represent important intermediate stages in the overall path. Intensities at all possible time points are compared, and τ values for all Δt values in a given time-resolved image series are calculated; Fig. 3 shows a representative example of this analysis for a 60-s trajectory.

From the fits to the temporal correlation curves for all image series, we found a resolvable distinction between two temporally distinct motion regimes: a short correlation period ($<$10 s) and a longer correlation period (noticeable by $\approx$60 s of correlation time for all data sets). The short correlation period was determined by fitting Eqs. **S8** or **S9** from *Supporting Methods* to the correlation traces and determining the time at which the velocity term was greater than the effective minimum detectable value of 0.01 μm/s (the limit of this setup). In most cases, this regime was for τ values of 10 s, and we chose 10 s as the short correlation period. The longer correlation period was determined by finding the times at which the correlation traces generally reached the minimum $g(0,0,\tau)$ value and leveled off for at least 10 s; this regime was for correlation times of $\approx$60 s. To confirm the existence of these two regimes, the data were additionally processed by using single-particle tracking (SPT) analysis (5); a more detailed comparison of ICS versus SPT and multiple-particle tracking is given in *Supporting Text*, which is published as supporting information on the PNAS web site. For 65 particles from three cells in the 100-nm PEI data set, the slope of the average mean square displacement curve was found to drop noticeably after 10 s correlation time, as previously determined from correlation analysis (Fig. 7, which is published as supporting information on the PNAS web site). From such analyses, we find that ICS is a useful and more rapid alternative to SPT for determining the average kinetic behavior of multiple intracel-

Table 1. Effective diffusion coefficients and velocity values for selected nonviral polyplexes for both short (10 s) and long (≈60 s) correlation times

	Short τ, 10 s		Long τ, ≈60 s	
Polyplex	*D* coefficient $\times 10^{-11}$ cm^2/s	Velocity, μm/s	*D* coefficient $\times 10^{-11}$ cm^2/s	Velocity, μm/s
Cyclodextrin, 80 nm ($n = 32$)	2.8 ± 0.8	0.049 ± 0.020	1.4 ± 0.6, $P < 0.0001$	0.007 ± 0.008, $P < 0.0001$
Cyclodextrin, 180 nm ($n = 14$)	3.2 ± 1.4	0.058 ± 0.021	1.8 ± 0.6, $P < 0.003$	0.008 ± 0.009, $P < 0.0001$
Cyclodextrin, 220 nm ($n = 16$)	4.4 ± 1.2	0.056 ± 0.034	2.2 ± 0.8, $P < 0.0001$	0.005 ± 0.007, $P < 0.0001$
PEI, 100 nm ($n = 38$)	3.1 ± 1.1	0.052 ± 0.031	1.6 ± 1.1, $P < 0.0001$	0.006 ± 0.009, $P < 0.0001$

The effective diffusion coefficients decrease somewhat for longer correlation times but the velocity terms (determined by fitting Eq. **S8** from *Supporting Methods*) are reduced by an order of magnitude to essentially zero. Values are reported as mean ± SD for the number of independent observations. *P* values are generated by comparing each parameter at short versus long τ values.

lular particles (Figs. 8 and 9, which are published as supporting information on the PNAS web site).

The polyplexes' motion was characterized by directed motion and diffusion on short time scales and mostly random motion on long time scales. Although both the effective diffusion and velocity values differed between the two correlation regimes, the velocity term showed the greatest variation (Table 1). Velocity values averaged 0.05 μm/s for short correlation times (for all polyplexes) and approached zero for longer correlation times. Effective diffusion terms ranged from 2.8 to 4.5 $\times$ 10^{-11} cm^2/s for short correlation times and from 1.4 to 2.2 $\times$ 10^{-11} cm^2/s for long correlation times. From the 100-s movies, we found that polyplex motion is highly variable and that shorter trajectories are not sufficient to fully characterize their behavior.

To confirm the role of microtubules in polyplex motion, nocodazole was added to the cells after allowing for internalization. Nocodazole is a drug that specifically causes microtubule depolymerization and would be expected to significantly hinder microtubule-dependent processes, including transport (4, 5). After addition, the motions of the polyplexes were dramatically reduced when compared with untreated cells (shown in Fig. 4*A*); three sample trajectories are shown in Fig. 4*B*. For a cell similar to one depicted in Fig. 4*B*, the effective diffusion coefficient was found to be 2.9 $\times$ 10^{-13} cm^2/s with no meaningful velocity term, 2 orders of magnitude smaller than for untreated cells. These nocodazole results illustrate the importance of microtubules for intracellular transport of polyplexes.

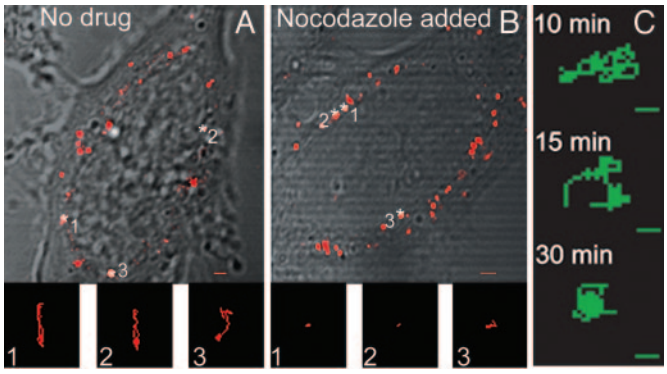

Fig. 4. The effects of nocodazole on intracellular directed transport. (*A*) One hundred-second trajectories of three 162-nm CD polyplexes in untreated cells. Although not all intracellular polyplexes are transported in this manner over the course of visualization, many will have directed motion for ≈10 s before stalling again, as demonstrated in these trajectories. (*B*) One hundred-second trajectories of three polyplexes in cells that were treated with nocodazole (final concentration 30 μM) after allowing polyplex uptake. These images were taken after 1 h of incubation in nocodazole. The three trajectories shown are representative of almost all particles seen in the cell; they do not exhibit directed motion as seen in *A*. The scale bars in *A* and *B* are 1 μm long. (*C*) Time course of nocodazole effect on polyplex trajectories. Representative trajectories are given after 10, 15, and 30 min of incubation in 30 μM nocodazole. The maximum trajectories of the polyplexes significantly decreases over time as the drug takes effect. (Scale bars: 0.5 μm.)

Implications of Two Temporal Fit Regimes. The idea of two temporal regimes of intracellular motion is not unique to this system; indeed, similar findings have been reported for μm beads moving in the cytoplasm and chromosome motion in the nucleus (34, 36, 37) describing random walk processes. The benefit of our analysis is that it provides information about the system while requiring minimal fit parameters. Polyplex movement depends on microtubule transport, and the two temporal regimes may also be described in terms of the activity of the microtubules and their motors (kinesin and dynein). For short intervals, the microtubule motors display a memory effect and are able to transport the polyplexes in a nonrandom, directed linear fashion. However, after this interval (which generally lasts up to 10 s), the motors may either pursue a different path or remain in place, and the correlation function decays further. Similar results have been reported by Caspi *et al.* (34, 36) for transport of μm-sized beads in cytoplasm. For short correlation times, the fits to the polyplex data yield an average velocity of 0.05 μm/s, independent of size or type; Ichikawa *et al.* (35) report similar values (0.05 μm/s) for endosomal motion. The velocity value represents an average of all particles within a region and not merely individual ones; it can also be thought of as an indirect measure of the activity of the microtubule motors.

This behavior is in contrast to polyplex motion at long correlation times; at long times the velocity term approaches zero when fit to Eqs. **S8** or **S9** from *Supporting Methods*. This result does not mean that the polyplexes are not transported, but rather the velocity vectors sum to almost zero and particle motion is reflected primarily by the diffusion term. Cumulatively, these data suggest that the particles have a "persistence time" over which transport motion is correlated and continues in that direction without much deviation. After that time, particle motion appears stochastic again. Direct visualization indicates that the directed behavior, during which the particles move a few microns, last for up to ≈10 s before the particle stalls or changes direction (Figs. 4*A* and 6). Over the image series, a given particle may not necessarily move far from its starting position. After many hours of motion, most polyplexes arrive in the perinuclear space.

Overall, the polyplexes exhibit a back-and-forth movement about their starting positions, similar to what has been reported for individual influenza viruses in one stage of their trajectories (5). This movement is caused by microtubule transport by both minus- and plus-end-directed motors (35). The persistence time can be related to the activities of the kinesin and dynein motors. For short periods of time, one group of motors predominates and the action of these motors propels the polyplex cargo (5). Competition between different motors oriented in all directions on the endosomal compartment as well as shifting of cargo

between different microtubule tracks causes the measured velocities to be lower than the maximal velocities reported for individual kinesin or dynein motors *in vitro* (38). We observed many instances of polyplexes being transported initially in one direction for up to 10 s and then appearing to be transferred to a neighboring microtubule track and moving along a different path. This process continues for several iterations until the particle stalls. This motion is the only type observed for these polyplexes; in contrast, influenza virus also displays a dynein-dependent, directional stage of motion (5).

Opposite to what might be expected, the effective diffusion terms increase with increasing size of the polyplexes. For instance, the 220-nm β-CD polyplexes (nominal diameter) have the largest effective diffusion constant (Table 1). As noted above, this term is only one component of intracellular motion because the particles are hindered by the crowded cytoplasm and cannot move freely. The velocity component, the major determinant of directed motion at short times, is not significantly different among the polyplexes at short times. Aside from the nominal diameter, it is the characteristics of the endosome, powered by kinesin and dynein, that primarily determine diffusion and velocity (4, 30, 35). Based on the average velocity measurements and effective diffusion constants for the τ values, we estimate that motor activity increases slightly with increasing endosome size.

The behavior of these polyplexes provides information about certain aspects of the intracellular environment, including microtubule transport. More generally, spatio-temporal ICS studies provide information about intracellular dynamics and other macromolecular characteristics. In comparison to multiple-particle tracking, ICS can extract a greater amount of data on a statistically broader basis. ICS can be used to assess the transport characteristics of modified polyplexes and their trafficking efficiencies relative to viruses or other DNA delivery systems or to analyze the relative importance of transport within the full pathway of polyplex delivery and gene expression. For example, polyplexes with attached ligands can be tested to determine which ligands increase transport velocities or whether chemical modifications increase nuclear delivery; this information will be useful in developing new agents that have increased transport and efficacy. Spatio-temporal ICS is a powerful technique for assessing the stochastic nature of this motion and calculating number densities, effective diffusion, and velocity values for all correlation times.

Conclusions

In this work, we have used spatio-temporal ICS to characterize the aggregate diffusion and velocity characteristics of intracellular polyplexes in real time. Using the standard fit equations described, these trajectories show a distinction between short and long correlation times, indicating that the motion of intracellular polyplexes is often vectorially directed for short periods of time (up to 10 s) but stochastic for longer periods; these motions depend on the activity of microtubule motors. Spatio-temporal ICS extends the power of fluorescence correlation spectroscopy into processes that occur on the time scale of many biological and cellular events, and it offers an overall picture of the dynamics in an intracellular environment. The dynamics of polyplexes described here should have general implications for the endocytic pathway and transport mechanisms for large (>30 nm) objects in the crowded cellular environment.

We thank Jeremy Heidel and Swaroop Mishra for assistance in making the polyplexes, Tania Demyanenko for assistance with tissue culture, and Mag Bak, Nils Petersen, Paul Wiggins, Paul Grayson, Michael Liebling, Helen McBride, Mary Dickinson, and Elaine Bearer for helpful discussion and comments on the manuscript. This work was supported by a National Institute of Child Health and Human Development grant (to S.E.F.) and a National Defense Science and Engineering Graduate Fellowship (to R.P.K.).

1. Roizman, B. (1996) *Proc. Natl. Acad. Sci. USA* **93,** 11307–11312.
2. Boussif, O., Lezoualc'h, F., Zanta, M. A., Mergny, M. D., Scherman, D., Demenix, B. & Behr, J. P. (1995) *Proc. Natl. Acad. Sci. USA* **92,** 7297–7301.
3. Luo, D. & Saltzman, W. M. (2000) *Nat. Biotechnol.* **18,** 33–37.
4. Suh, J., Wirtz, D. & Hanes, J. (2003) *Proc. Natl. Acad. Sci. USA* **100,** 3878–3882.
5. Lakadamyali, M., Rust, M. J., Babcock, H. P. & Zhuang, X. (2003) *Proc. Natl. Acad. Sci. USA* **100,** 9280–9285.
6. Gerlich, D., Beaudouin, J., Gebhard, M., Ellenberg, J. & Eils, R. (2001) *Nat. Cell. Biol.* **3,** 852–855.
7. Luby-Phelps, K., Castle, P. E., Taylor, D. L. & Lanni, F. (1987) *Proc. Natl. Acad. Sci. USA* **84,** 4910–4913.
8. Lukacs, G. L., Haggie, P., Seksek, O., Lechardeur, D., Freedman, N. & Verkman, A. S. (2000) *J. Biol. Chem.* **275,** 1625–1629.
9. Verkman, A. S. (2002) *Trends Biochem. Sci.* **27,** 27–33.
10. Seksek, O., Biwersi, J. & Verkman, A. S. (1997) *J. Cell Biol.* **138,** 131–142.
11. Arrio-Dupont, M., Foucault, G., Vacher, M., Devaux, P. F. & Cribier, S. (2000) *Biophys. J.* **78,** 901–907.
12. Forrest, M. L. & Pack, D. W. (2002) *Mol. Ther.* **6,** 57–66.
13. Ellis, R. J. & Minton, A. P. (2003) *Nature* **425,** 27–28.
14. Ellis, R. J. (2001) *Trends Biochem. Sci.* **26,** 597–604.
15. Petersen, N. O., Hoddelius, P. L., Wiseman, P. W., Seger, O. & Magnusson, K.-E. (1993) *Biophys. J.* **65,** 1135–1146.
16. Magde, D., Elson, E. L. & Webb, W. W. (1972) *Phys. Rev. Lett.* **29,** 705–708.
17. Elson, E. L. & Magde, D. (1974) *Biopolymers* **13,** 1–27.
18. Magde, D., Elson, E. L. & Webb, W. W. (1974) *Biopolymers* **13,** 29–61.
19. Kettling, U., Koltermann, A., Schwille, P. & Eigen, M. (1998) *Proc. Natl. Acad. Sci. USA* **95,** 1416–1420.
20. Schwille, P., Haupts, U., Maiti, S. & Webb, W. W. (1999) *Biophys. J.* **77,** 2251–2265.
21. Schwille, P., Korlach, J. & Webb, W. W. (1999) *Cytometry* **36,** 176–182.
22. Wachsmuth, M., Waldeck, W. & Langowski, J. (2000) *J. Mol. Biol.* **298,** 677–689.
23. Petersen, N. O. (1986) *Biophys. J.* **49,** 809–815.
24. Thompson, N. L., Lieto, A. M. & Allen, N. W. (2002) *Curr. Opin. Struct. Biol.* **12,** 634–641.
25. Rocheleau, J. V., Wiseman, P. W. & Petersen, N. O. (2003) *Biophys. J.* **84,** 4011–4022.
26. Huang, Z. & Thompson, N. L. (1996) *Biophys. J.* **70,** 2001–2007.
27. Srivastava, M. & Petersen, N. O. (1996) *Methods Cell Sci.* **18,** 47–54.
28. Wiseman, P. W., Squier, J. A., Ellisman, M. H. & Wilson, K. R. (2000) *J. Microscopy* **200,** 14–25.
29. Wiseman, P. W., Brown, C. M., Webb, D. J., Hebert, B., Johnson, N. L., Squier, J. A., Ellisman, M. H. & Horwitz, A. F. (2004) *J. Cell. Sci.* **117,** 5521–5534.
30. Mishra, S., Webster, P. & Davis, M. E. (2004) *Eur. J. Cell Biol.* **83,** 97–111.
31. Saxton, M. J. & Jacobson, K. (1997) *Annu. Rev. Biophys. Biomol. Struct.* **26,** 373–399.
32. Lidke, D. S., Nagy, P., Heintzmann, R., Arndt-Jovin, D. J., Post, J. N., Grecco, H. E., Jares-Erijman, E. A. & Jovin, T. M. (2004) *Nat. Biotechnol.* **22,** 198–203.
33. Hasegawa, S., Hirashima, N. & Nakanishi, M. (2001) *Gene Ther.* **8,** 1669–1673.
34. Caspi, A., Granek, R. & Elbaum, M. (2000) *Phys. Rev. Lett.* **85,** 5655–5658.
35. Ichikawa, T., Yamada, M., Homma, D., Cherry, R. J., Morrison, I. E. G. & Kawato, S. (2000) *Biochem. Biophys. Res. Commun.* **269,** 25–30.
36. Caspi, A., Granek, R. & Elbaum, M. (2002) *Phys. Rev. E* **66,** 011916-12.
37. Vazquez, J., Belmont, A. S. & Sedat, J. W. (2001) *Curr. Biol.* **11,** 1227–1239.
38. Suomalainen, M., Nakano, M. Y., Keller, S., Boucke, K., Stidwill, R. P. & Greber, U. F. (1999) *J. Cell. Biol.* **144,** 657–672.